JOURNAL DE PHYSIQUE IV
Colloque C1, supplément au Journal de Physique III, Volume 6, janvier 1996

Modelling of Electromagnetic Heating, Cooling and Phase Transformations during Surface Hardening of Steels

A. Jacot, M. Swierkosz*, J. Rappaz*, M. Rappaz and D. Mari**

Ecole Polytechnique Fédérale de Lausanne, Laboratoire de Métallurgie Physique, MX-G, 1015 Lausanne, Switzerland
** Ecole Polytechnique Fédérale de Lausanne, Département de Mathématiques, 1015 Lausanne, Switzerland*
*** AMYSA Yverdon SA, 1400 Yverdon, Switzerland*

A comprehensive micro-macroscopic model of the continuous hardening of 3d-axisymmetric steel components by induction heating has been developed. At the macroscopic scale, the Maxwell and heat flow equations are solved using a mixed numerical formulation : the inductor and the workpiece are enmeshed with finite elements (FE) but boundary elements (BE) are used for the solution of the electromagnetic equations in the ambient air. This method allows the inductor to be moved with respect to the workpiece without any remeshing procedure. The heat flow equation is solved for the workpiece using the same FE mesh. For the thermal boundary conditions, a net radiation method has been implemented to account for grey diffuse bodies and the viewing factors of the element facets are calculated using a "shooting" technique. The boundary condition associated with the water spraying below the inductor is deduced from the inverse modelling of temperatures measured at various locations of a test piece. These macroscopic calculations of induction heating have been coupled to a microscopic model describing the solid state transformations that occur during both heating and cooling. From the local thermal history, the evolutions of the various phase fractions are predicted from TTT-diagrams using an additivity principle. A micro-enthalpy method has been implemented in the heat flow calculations in order to account for the latent heat released by the various transformations. At each time step the local properties of the material, in particular its magnetic susceptibility, are updated according to the new temperatures and magnetic field. The results of the simulation are compared with experimental cooling curves and hardness profiles.

1. INTRODUCTION

Induction techniques are increasingly used in various industrial applications related to material processes [1] (e.g., magnetic stirring of continuously cast steel slabs, electromagnetic semi-continuous casting of aluminium alloys, skull melting, levitation, induction heating, etc.). Among them, stream induction heating and quenching of steel components plays an important role : it allows to keep the ductility of the bulk material while improving the hardness of the surface over a well-controlled depth [2]. In this process, an inductor moves vertically along the workpiece to be hardened and induces eddy currents over the skin depth (Fig. 1). The associated heating (Joule effect) partially or fully transforms the ferrito-perlitic structure into austenite. A water spraying system attached below the inductor then induces solid-state transformations upon rapid cooling conditions, thus providing a hardening of a surface layer.
Modelling of the stream induction/quenching process allows us to optimize the heating and cooling conditions as a function of the geometry of the piece and of the desired mechanical properties. It is a challenge because it involves several physical phenomena which are partially coupled. The Maxwell equations and Ohm's law have to be solved first for a geometry which varies with time, since the inductor

moves with respect to the workpiece. This provides a source term for the heat diffusion equation which adds to the latent heat associated with the various transformations. The phase transformations themselves are directly coupled to the heating and cooling conditions (and to some extent to the induced thermal and transformation strains). Radiation at the free surface and heat extraction from a turbulent water spray have also to be accounted for. Finally, the temperature variations and the evolutive phase fractions clearly affect the electromagnetic and thermophysical properties.

Modelling of solid-state phase transformations has been studied by many authors [3-12]. The present approach uses some of the knowledge which has been gathered during these studies (e.g., additivity principle [6,7,8,11]) in a fully integrated model of induction-conduction-radiation-transformation (ICRT). The model relies on a mixed finite element (FE) - boundary element (BE) formulation for the solution of the electromagnetic problem [13] and on a micro-enthalpy method for the solution of the coupled heat flow equation and phase transformations [14]. The results provided by the model are compared with cooling curves and hardness profiles measured for Ck45 steel cylinders.

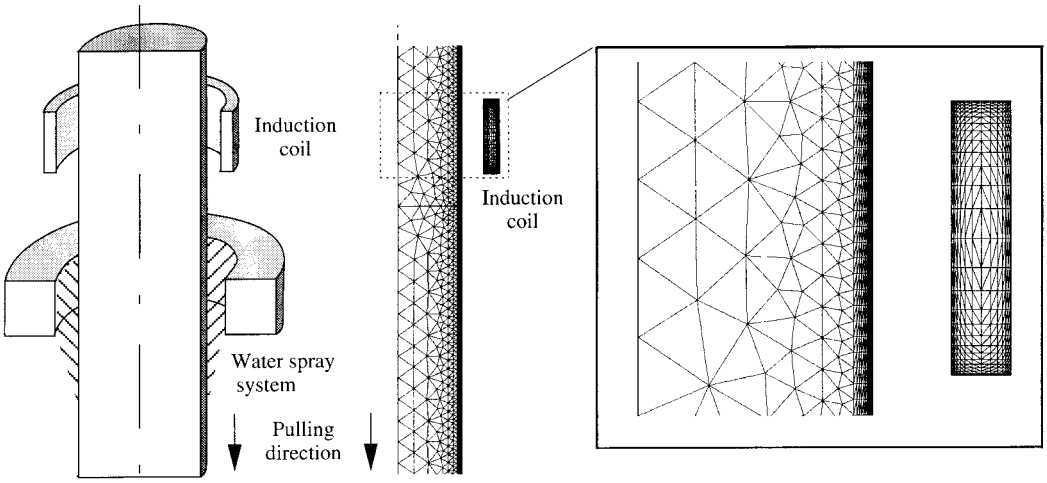

Figure 1 : Schematic view of a cylindrical piece which is induction heated and then quenched. For symmetry reasons, only one half of the longitudinal section of the cylinder and induction coil is enmeshed with finite elements; the boundary element formulation provides a coupling between these two conductive media.

2. DESCRIPTION OF THE MODEL

2.1 Induction heating

In order to predict the heat generated by the induced electric currents, the Maxwell equations have to be solved first for an axisymmetric geometry. The vectors $\mathbf{e}_r$, $\mathbf{e}_\theta$, and $\mathbf{e}_z$ are the usual basis vectors of the cylindrical coordinate system, where $\mathbf{e}_z$ is the vertical axis of the axisymmetric piece. An alternating voltage, V_E, is applied to the inductor and the current flowing within this conductor is assumed to be sinusoidal and along $\mathbf{e}_\theta$. Under such conditions, it can be shown that the magnetic induction field, **B**, has non-zero components along $\mathbf{e}_r$ and $\mathbf{e}_z$ only. It can be expressed in terms of a scalar potential $\phi(r,z)$ as [13] :

$$\mathbf{B} = \mathbf{curl}\ (\phi\ \mathbf{e}_\theta)\ . \qquad (1)$$

Combining the Maxwell equations with Ohm's law yields the following equation for $\phi(r,z)$ inside the conductive media (workpiece and coil) :

$$-\left[\frac{\partial}{\partial r}\left(\nu\frac{\partial(r\phi)}{\partial r}\right)+\frac{\partial}{\partial z}\left(\nu\frac{\partial\phi}{\partial z}\right)\right]+i\sigma\omega\phi=\sigma\frac{V_E}{2\pi r}. \qquad (2)$$

Electrical conductivity is denoted by σ, ν is the inverse of the magnetic permeability, and ω is the circular frequency of the current. Outside these two media, a similar equation can be written accounting for the fact that the current $\mathbf{j}$ equals zero and that ν is constant. One gets $\Delta[\phi\mathbf{e}_\theta] = 0$ and so :

$$\left[\frac{\partial}{\partial r}\left(\frac{1}{r}\frac{\partial(r\phi)}{\partial r}\right)+\frac{\partial^2\phi}{\partial z^2}\right]=0. \qquad (3)$$

Suitable interface conditions have to be written at the boundary of the conductors. Equation (2) can be solved using a finite element method but equation (3) cannot for two reasons : first, the external domain (air) is unbounded and second, this domain varies with time due to the motion of the inductor with respect to the workpiece. Accordingly, equation (3) is rewritten into the equivalent form :

$$\Delta[\phi(r,z)\cdot\sin\theta]=0. \qquad (4)$$

Using a simple-double layer representation on the boundary, we use equation (4) to express the magnetic potential outside the conductors [13]. This finite element - boundary element model yields the magnetic potential and subsequently the eddy current density inside the workpiece. The finite element part accounts for the behaviour of the electromagnetic field inside the conductors (inductor and workpiece), while the boundary element part stands for the behaviour of the electromagnetic field in the ambient air, providing thus a coupling between the inductor and the workpiece. Details of this formulation can be found in [13].

2.2 Diffusion and radiation

In order to predict the phase transformations that occur during the heat treatment, the temperature field has to be known at each time-step. This is achieved by solving the heat-diffusion equation :

$$\text{div}\,(\kappa\,\mathbf{grad}\,T(\mathbf{x},t))+\dot{Q}(\mathbf{x},t)=\frac{\partial h(\mathbf{x},t)}{\partial t}, \qquad (5)$$

where κ is the thermal conductivity, $\dot{Q}$ a source term and h the volumetric enthalpy. The solution of this equation using the FEM software code *3-MOS* * is based upon an implicit scheme, an enthalpy formulation and a Newton-Raphson iterative technique [14]. Accordingly, the latent heat associated with the various phase transformations is integrated directly within the enthalpy term, h. This scheme ensures the energy conservation without any special treatment. The heat source term, $\dot{Q}$, is directly given by $|\mathbf{j}|^2/\sigma$ where $\mathbf{j}$ is the density current obtained from the resolution of the electromagnetic problem.
Among the various types of boundary conditions that can be used in the software *3-MOS*, radiative heat transfer is particularly useful since the temperature of the workpiece surface, T_S, can be quite high. Making the assumption of grey diffuse surfaces, the radiative loss of convex workpieces can be estimated easily from the Stefan-Boltzmann law :

$$q = \varepsilon\cdot\sigma_B\cdot(T_S^4 - T_O^4), \qquad (6)$$

where T_O is the ambient temperature, q the radiated thermal flux, ε the relative emissivity of the surface and σ_B the Stefan-Boltzmann constant. However, modelling the radiation for concave grey bodies is much more difficult since the emitted radiation can be reflected and partially absorbed by other surfaces of the

* *3-MOS* is a software developed at EPFL and diffused through the company Calcom SA, Lausanne, Switzerland.

workpiece. The problem can be solved using the net radiation method [15]. In this technique, the surface of the workpiece is subdivided into a large number of small facets - usually the intersection of the finite elements with the boundary - whose temperature is assumed to be uniform (e.g., considered to be equal to the average of the temperatures at the nodal points of the considered FE facet). The net heat flux, q_i^{out}, coming out from facet i includes the radiation which is reflected by the facet and the radiated energy itself :

$$q_i^{out} = (1-\varepsilon_i)\cdot q_i^{in} + \varepsilon_i \sigma_B T_i^4 ; \qquad (7)$$

q_i^{in} is the incoming radiation and the reflectivity is assumed to be equal to $(1-\varepsilon_i)$ (i.e., absorptivity equal to the emissivity). The incoming flux, q_i^{in}, is the sum of the fluxes coming out from all the other facets j (including the ambient air which is considered as one global facet) multiplied by the corresponding viewing factors, F_{ij} [15] :

$$q_i^{in} = \sum_{j \neq i} F_{ij}\, q_i^{out} . \qquad (8)$$

The F_{ij} coefficients are geometrical factors depending on the relative position of each pair of "viewing" facets i and j. For axisymmetric geometries, these factors have to be calculated in 3 dimensions since each FE edge in a longitudinal section corresponds in fact to a portion of a cone*. A shooting technique was especially conceived to calculate these coefficients [16]. Combining equations (7) and (8) for all the facets finally yields a set of linear equations :

$$[A]\cdot\mathbf{q}^{out} = \mathbf{b} , \quad \text{with } b_i = \frac{\varepsilon_i}{1-\varepsilon_i}\sigma_B T_i^4 \quad \text{and} \quad \begin{cases} A_{ij} = \dfrac{1}{1-\varepsilon_i} & \text{if } i = j , \\ A_{ij} = -F_{ij} & \text{if } i \neq j . \end{cases} \qquad (9)$$

This set of equations describing the radiation among all the facets is solved at each time step of the diffusion equation using the known (explicit) temperatures. Once these radiative heat fluxes are known, the boundary condition used in the diffusion equation for each facet is the following :

$$\kappa \frac{\partial T}{\partial n} = q_i^{in} - q_i^{out} - \alpha\cdot(T - T_o) = \frac{\varepsilon_i}{1-\varepsilon_i}\left(q_i^{out} - \sigma_B T_i^4\right) - \alpha\cdot(T_i - T_o) . \qquad (10)$$

The possible convective heat transfer with the ambient air has been modelled via a heat transfer coefficient α.

2.3 Phase transformations

The kinetics of the phase transformations that can occur during local heating and cooling of the workpiece is calculated using the well-known Avrami [17] or Johnson-Mehl [18] equation :

$$f_k = f_k^{max}(T)\cdot\left[1 - \exp(-b_k(T)\cdot t^{*n})\right] , \qquad (11)$$

where f_k is the volume fraction of the phase k (k = ferrite, pearlite, austenite, bainite), $b_k(T)$ is a temperature-dependent parameter and n is a parameter that describes the nucleation and growth mechanisms. It has been fixed to 3, a value that corresponds to the assumption of instantaneous nucleation. The maximum (equilibrium) volume fraction of the phase k that can form at the temperature T is denoted by $f_k^{max}(T)$. The temperature dependence of the parameters b_k has been determined from the two "C-curves" (start and end) of the TTT-diagram [19] using a least squares method.

---

* If the edge is vertical or horizontal, the surface degenerates to a portion of a cone or to an annulus, respectively.

The cooling or heating curve at a given mesh point of the workpiece is subdivided into small isothermal steps (see Fig. 2) in order to be able to use the TTT diagram information and the additivity principle [7,8]. The basic principle of this technique, which is illustrated in Fig. 3, can be summarized as follows : on each small isothermal step, the kinetics equation (11) is applied as if the transformation had always been at this temperature and had reached the same volume fraction f_k. This requires to introduce a fictitious time, t_i^*, in order to obtain a fraction of phase at the beginning of the time step i, which is equal to the one previously calculated at the end of the previous time step, (i-1). This fictitious time (which in fact depends also on the phase k being considered) is given by :

$$t_i^* = \left[\frac{1}{b_k(T_i)} \, Ln \left(\frac{f_{k,i}^{max}}{f_{k,i}^{max} - f_{k,i-1}} \right) \right]^{1/n} . \qquad (12)$$

The new volume fraction at the end of the time step i is then determined by adding the time step to the virtual time t_i^* :

$$f_{k,i} = f_{k,i}^{max} \cdot \left[1 - \exp\left(-b_k(T_i) \cdot (t_i^* + \Delta t)^n \right) \right] . \qquad (13)$$

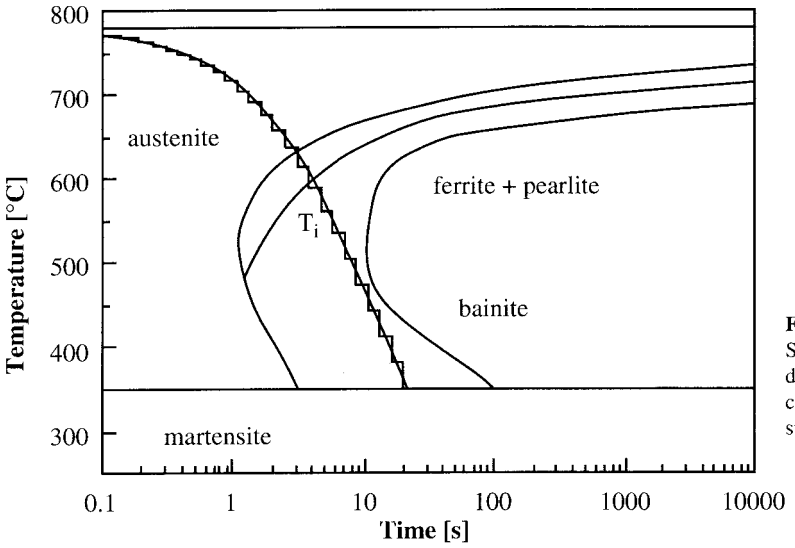

Figure 2 :
Schematic view of the TTT diagram of Ck45 steel and of a cooling curve decomposed into small isothermal plateaus.

The austenite remaining at M_s (martensite start temperature) is partially transformed into martensite according to Koistinen and Marburger's law [20] :

$$f_\gamma = \exp\left[-\beta(M_s - T) \right] , \qquad (14)$$

where β is a constant and f_γ the volume fraction of residual austenite.
When the volume fractions of the different phases formed during the heat treatment are known, the local hardness of the materials, H_V, can be calculated according to the mixture rule proposed by Denis et al [8] :

$$H_V = \sum_i \sum_k \Delta f_{k,i} \, H_{V_{k,i}} , \qquad (15)$$

where $\Delta f_{k,i}$ and $H_{V_{k,i}}$ are the volume fraction and the microhardness of the phase k that has formed at temperature or time step, i, respectively.

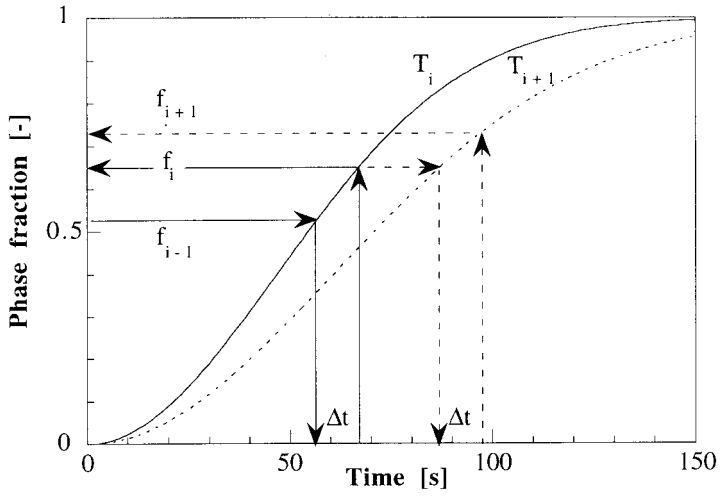

Figure 3 : Additivity principle used for the phase transformation calculations based upon TTT diagrams.

2.4 Coupling

The overall flow chart of the simulation software described in the previous sections is illustrated in Fig. 4. Before starting the main time step loop, several entities are initialised or calculated, in particular the viewing factors of radiation, F_{ij}, and the fixed boundary integrals appearing in the electromagnetic calculations (self-induction of each conductive medium). The various operations performed then at each time step are as follows :

- The workpiece is moved vertically by an increment $v \cdot \Delta t$, where v is the displacement rate and Δt the time step.
- The variable boundary integrals (i.e., the ones that correspond to the coupling between the workpiece and the induction coil) are calculated for this new position of the workpiece.
- The electromagnetic problem is then solved in the new configuration, thus providing the magnetic field, **H**, everywhere and the current density **j** within the workpiece and induction coil.
- Once the Joule effect term, $\dot{Q} = \mathbf{j}^2/\sigma$ is known, the heat flow equation and the phase transformation calculations are performed iteratively in order to account for the associated latent heat release. The explicit (i.e., known) temperatures and enthalpy variations calculated at each FE nodal point using a Newton-Raphson linearization scheme are given as input to the metallurgical module. The latter then calculates the new volume fractions of each phase using a "microscopic" time step smaller than the one used in the FE heat flow calculation. This two-time-step procedure is necessary since the phase transformations near the surface of the workpiece (i.e., fast heating and cooling rates) can be completed in less than 10 "macroscopic" time steps. The latent heat of the different phase transformations is then used to calculate the new temperatures and the procedure is repeated until convergence is reached.
- At the end of each time step, the physical properties (thermal conductivity κ, specific heat ρCp, electrical conductivity σ and magnetic susceptibility ν^{-1}) are updated according to the new temperatures and magnetic field.

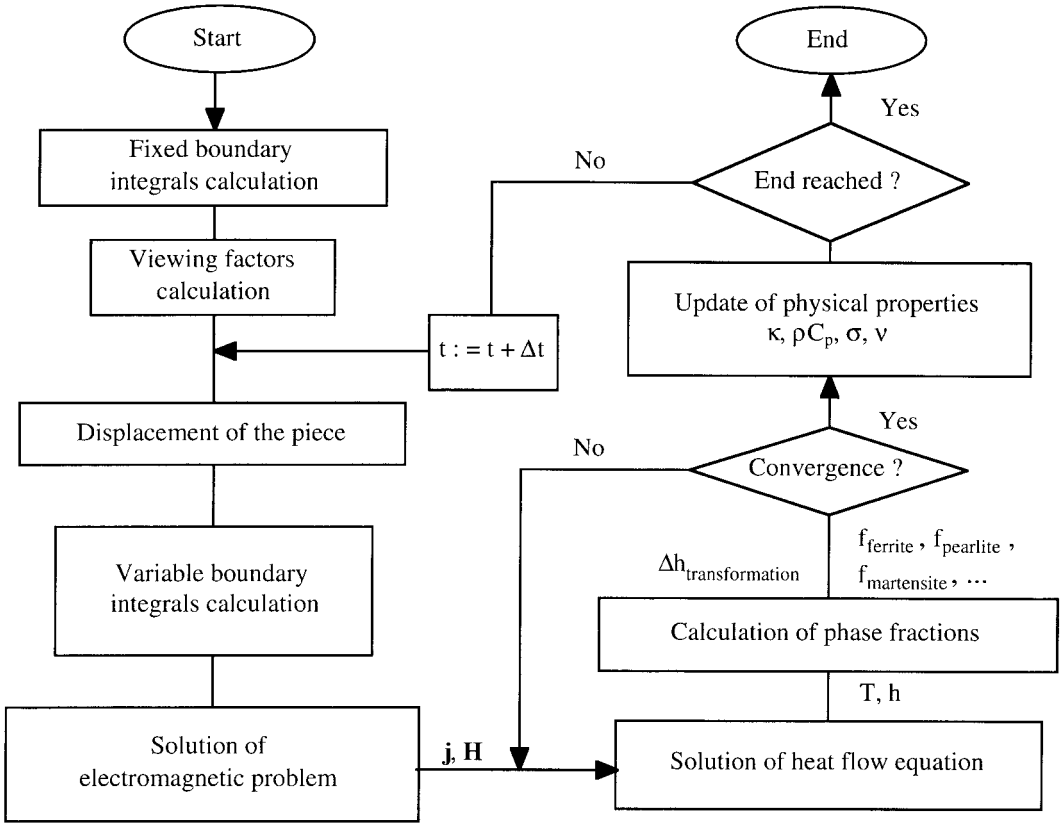

Figure 4 : Flow chart of the stream quenching simulation program

3. APPLICATION OF THE MODEL

3.1 Stream heating experiment

A stream heating experiment without quenching was first performed in order to validate the electromagnetic calculations. After a short period (0.8 s) of preheating, the induction coil was moved downwards along a cylindrical workpiece at a velocity of 5 mm/s. A sinusoidal variable current with a 10 kHz frequency was applied; the voltage was about 40 V. The workpiece made out of Ck45 carbon steel was simply cooled down by natural convection in air. Several thermocouples were placed inside the cylinder as indicated in the small insert of Fig. 5. A numerical simulation was then performed according to the same specifications. Fig. 5 shows a comparison between the calculated and measured temperatures. It should be pointed out that the temperature measurements are performed in presence of electromagnetic field. This may have an effect on thermocouples lying on the sample surface. On the other hand, the thermocouples lying beyond the skin depth are screened from electromagnetic influence. Indeed, discrepancies between simulated and experimental data are found in measurements close to the sample surface. Furthermore, the size of the thermocouple holes (about 1 mm) is quite large considering the high temperature gradient in the workpiece near the surface (typically 100 K/mm). Therefore, it can be concluded that the discrepancies between experimental and simulated temperature curves are within the experimental errors.

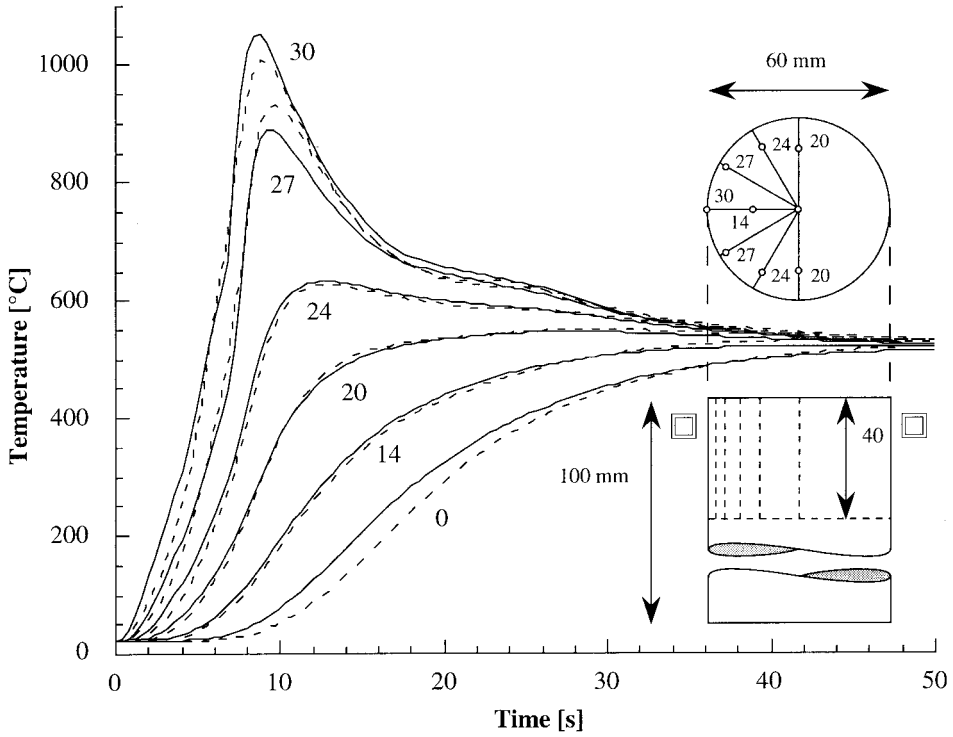

Figure 5 : Measured (dashed lines) and calculated (continuous lines) temperatures during stream induction heating of a 60 mm diameter CK45 steel cylinder (10 kHz, 40 V, 5 mm/s). The small insert shows the position of the thermocouples; the numbers indicate their radial distance in mm.

3.2 Stream quenching

The simulation software was then applied to the situation of stream quenching schematically shown in Fig. 1. This situation introduces a new parameter, and difficulty, into the simulation : the heat extracted by the water cooling system. This boundary condition was modelled via the use of a temperature-dependent heat transfer coefficient whose tabulated values were determined using inverse models [21]. For that purpose, separate measurements of temperatures were made during water spray cooling under static conditions (i.e., the shower was not moved). The results of such calculations are shown in Fig. 6 where the tabulated values of the heat transfer coefficient are reported as a function of the surface temperature of the workpiece for three water flow rates. The stream quenching experiment itself was performed on a 12 mm diameter Ck45 steel cylinder. The enmeshment of both the workpiece and induction coil is shown in Fig. 1. The conditions of these experiments were as follows : pulling speed 4 mm/s, applied voltage 25 V and frequency 700 kHz. The long cylinder used in these experiments (120 mm) had an aspect ratio which ensured nearly steady-state conditions for the temperature and electromagnetic fields, and thus for the phase distribution, at mid-height of the stream quenching experiment. Fig. 7 shows the calculated temperature field (left) and phase distribution (right), at nearly steady state as well as the position of the induction coil (small rectangle). An austenitic zone can be observed near the surface below the induction coil, while the core of the workpiece remains ferrito-perlitic. The austenitic region formed during heating then transforms into martensite upon rapid water cooling (lower area on Fig. 7). The two lines separating the labelled zones delimit the transient regions where several phases are present. The fraction of each of

them was calculated according to the method described in Section 2.3 but was not represented for the sake of clarity. Based upon the various phases present, the local hardness of the workpiece was calculated using Eq. (15) and the nominal hardness reported in the literature for each phase [19]. The simulated hardness profile is compared with the values measured actually in the workpiece in Fig. 8. It can be observed that the agreement is fairly good, a martensitic region of about 0.8 mm depth being observed on both curves.

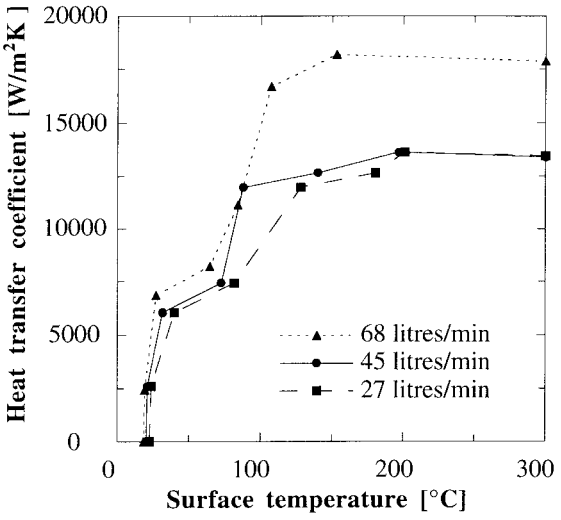

Figure 6 :
Heat transfer coefficient characterizing the water shower at various flow rates as a function of the surface temperature of the piece. These points were obtained from the temperatures measured in an axisymmetric piece using an inverse modelling technique [21].

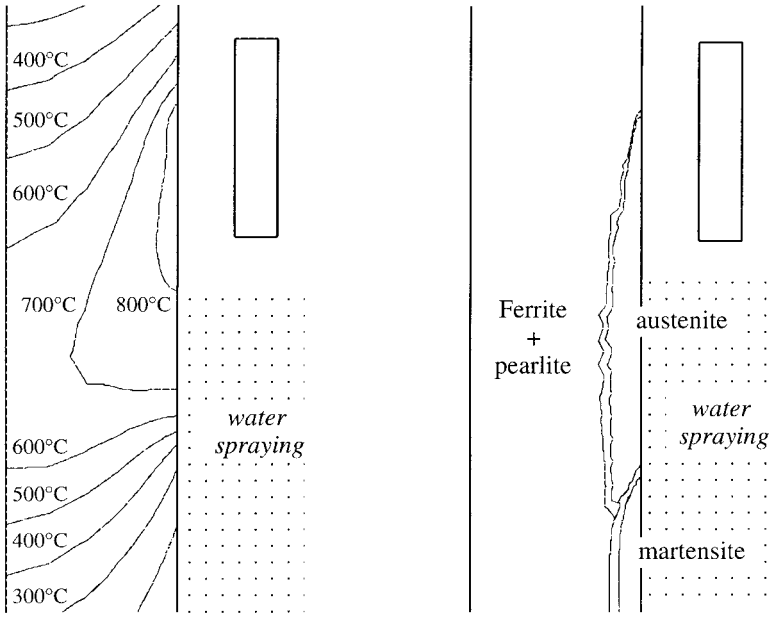

Figure 7 : Nearly steady-state isotherms (left) and phase distribution (right) in a 12 mm diameter Ck45 steel cylinder being stream quenched (700 kHz, 25 V, 4 mm/s).

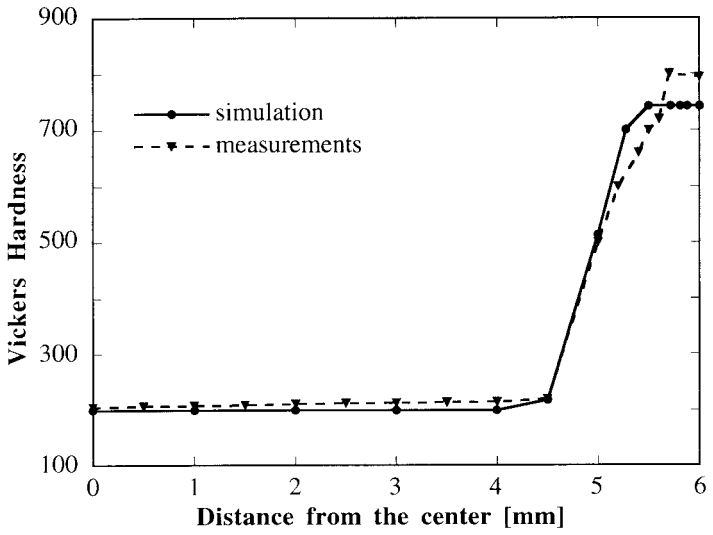

Figure 8 : Measured (dashed line) and calculated (continuous line) hardness profiles in a Ck45 steel cylinder which has been stream quenched (same conditions as for Fig. 7).

4. CONCLUSION

The results shown in the present paper demonstrate the utility of a combined induction-diffusion-radiation-transformation (ICRT) model for the prediction of temperatures and microstructures in processes involving induction heating. The model is certainly quite unique in the sense that it combines in a global approach various aspects essential for the process : a mixed FE-BE electromagnetic formulation which allows the workpiece to be moved with respect to the induction coil without remeshing, a two-time-step enthalpy formulation able to account for the latent heat released by the various phase transformations, a net radiation method, an inverse modelling determination of the heat transfer condition associated with the water spraying and finally a coupling with TTT diagrams using an additivity principle. All of these aspects have been validated separately in order to obtain a good correspondence with carefully controlled experiments so that the model can now be used for unknown situations with some confidence.

ACKNOWLEDGEMENTS

The authors would like to acknowledge the Commission pour l'Encouragement de la Recherche Scientifique, Bern, (CERS Grant 2568.2), the Nationaler Energieforschungsfonds, Basel, (NEFF Grant 497) and the companies Amysa-Yverdon SA, Yverdon, Bobst SA, Prilly, and Calcom SA, Lausanne, for the financial support and Mr A. Gillieron of the EINEV, Yverdon, for providing stream quenching data.

REFERENCES

1. E. J. Davies, *Conduction and Induction Heating*, P. Peregrinus (1990).
2. C. Chaboudez, S. Clain, R. Glardon, J. Rappaz, M. Swierkosz and R. Touzani, IEEE Trans. on Magnetics **30**, 5028 (1994).
3. *Recent Advances in Modelling on Microstructural Evolution and Properties of Steels*, ISIJ Intern. **32** (1992).
4. H.K.D.H. Badheshia, L.-E. Svensson and G. Gretoft, Acta Metall. **33**, 1271 (1985).
5. M. Enomoto, in ref. 3, p. 297.
6. E. Scheil, Arch. Eisenhuttenwesen **12**, 565 (1935).
7. J. W. Christian, *Theory of Transformation in Metals and Alloys*, Part 1, 2nd ed., Pergammon Press, Oxford, 1975.
8. S. Denis, D. Farias et A. Simon, in ref. 3, p. 316.
9. F. Fernandez, S. Denis and A. Simon, Mém. Etud. Sci. Rev. Métall. **83**, 355 (1986).
10. P. K. Agarval and J.K. Brimacombe, Met. Trans. **12B**, 121 (1981).
11. M. Umemoto, Trans. ISIJ **23**, 695 (1981).
12. J. B. Leblond and J. Devaux, Acta Metall. **32**, 137 (1984).
13. S. Clain, J. Rappaz and M. Swierkosz, in *Finite Element Method: Fifty Years of the Courant Element*, proceedings of the FEM-50 Conference, Jyväskylä (Finland), 1993.
14. Ph. Thévoz, M. Rappaz and J.-L. Desbiolles, in *Light Metals*, Ed. Ch. M. Bickert (The Minerals, Metals and Materials Soc., 1990), p. 975.
15. R. Siegel and J.R. Howell, *Thermal Radiation Heat Transfer*, (Hemisphere Publishing Corporation, New York, 1982) p. 306-318.
16. Ibid. p.187.
17. M. Avrami, J. Chem. Phys. **8**, 212 (1940).
18. W. A. Johnson and R. F. Mehl, Trans. Am. Inst. Min. Engrs **135**, 416 (1939).
19. *Atlas zur Wärmebehandlung der Stahle*, Verlag Stahleise GmbH, Düsseldorf, 1954.
20. D.P. Koistinen and R.E. Marburger, Acta Met. **7**, 59 (1959).
21. M. Rappaz, J.-L. Desbiolles, J.-M. Drezet, Ch.-A. Gandin, A. Jacot and Ph. Thévoz, in : *Modeling of casting, welding and advanced solidification processes VII* (TMS, Warrendale, Pennsylvania, 1995). To appear.